Full Paper Transactions, SMiRT 28
Toronto, Canada, August 10-15, 2025

FLUID-STRUCTURE-SOIL INTERACTION ANALYSIS FOR STEEL-CONCRETE COMPOSITE STRUCTURES TAKING INTO ACCOUNT NONLINEAR STRUCTURAL BEHAVIOR BASED ON JAPANESE AND US STANDARDS

Yuki Sato[1,2], Dan M. Ghiocel[3], Shunji Kataoka[4], Issei Ota[5], and Yasutomi Morimoto[6]

[1] Senior Project Engineer, JGC Corporation, Kanagawa, Japan (sato.yuuki@jgc.com)
[2] Ph.D Student, The University of Tokyo, Tokyo, Japan (yukisato@g.ecc.u-tokyo.ac.jp)
[3] President, Ghiocel Predictive Technologies, Inc., New York, USA (dan.ghiocel@ghiocel-tech.com)
[4] Principal Engineer, JGC Corporation, Kanagawa, Japan (kataoka.shunji@jgc.com)
[5] Engineer, JGC Corporation, Kanagawa, Japan (ota.issei@jgc.com)
[6] Senior Project Manager, JGC Corporation, Kanagawa, Japan (morimoto.yasutomi@jgc.com)

ABSTRACT

This paper presents a case study of the Fluid-Structure-Soil Interaction (FSSI) analysis for Steel-concrete Composite (SC) structure considering inelastic deformation of the SC structure using both Japanese and US standards. In some nuclear related buildings, large water mass is contained in the buildings, such as spent fuel pools. Since the interaction of the water and structure provides a significant effect on the structure, this study adopts FSSI analysis following the study (Sato, et.al, 2024). Additionally, the structure inelastic behavior was also considered since it is one of the important factors for structures in high seismic regions. However, how to treat the inelasticity of SC structures differs from design code to design code. The objective of this study is to evaluate how the differences in the inelastic modeling approaches used the Japanese and US codes could affect the seismic responses of SC structures under severe earthquakes. In this study, the FSSI analyses were performed for a typical nuclear related building with deep embedment in accordance with Japanese and US design codes. The FSSI analysis results show very similar seismic responses for the two design codes application, although the seismic input has 1G maximum ground acceleration. This is mainly due to the highly robust design of the selected nuclear building with high resistance SC walls. Detailed comparisons are shown in the in-structure response spectra (ISRS).

FSSI ANALYSIS APPROACH FOR DEEPLY EMBEDDED STRUCTURES

The seismic analysis has been performed for a deeply embedded nuclear building with consideration of Soi-Structure Interaction (SSI) effects. The SSI analysis adopts complex frequency response method using the ACS SASSI NQA Version 4.3.7 commercial software with the Flexible Volume Reduced-Order Modeling Approaches, briefly FVROM (Ghiocel Predictive Technologies, Inc., 2023).

With regard the Fluid-Structure Interaction, the ACS SASSI Option AA-F has been applied to the fluid pool structure. The dynamic behavior of the fluid is calculated in ANSYS as FLUID80 elements, and the calculated matrix forms are applied to the fluid elements of the ACS SASSI as a function of option AA-F (Sato et al., 2023). The FSSI effects can be treated as the combination of the above the SSI and FSI effects.

SAMPLE BUILDING STRUCTURE MODEL AND GENERIC SITE CONDITIONS

The building structure Finite Element model for this study is shown in Figure 1. The height of the building is 31 m with the embedment of 12m. The outer dimensions are 29.4 m x 19.4 m for each X and Y direction. The soil layers were assumed as uniform layer with the shear wave velocity, Vs =800 m/s. In the building model, all structure walls were modeled as SC walls. The floor slabs are modeled as reinforced concrete (RC) components.

The seismic motion input for the SSI analysis is shown in Figure 2. The surface ground motions were generated to fit the target design spectrum that is identical with the NuScale CSDRS (Certified Seismic Design Response Spectra) (NuScale Power, LLC., 2020). In the FSSI analysis, the maximum ground surface acceleration was scaled to be 1.0 G for horizontal direction and 0.8 G for vertical direction.

The large 1G ground acceleration was considered for investigating the effects of the SC structure nonlinear behavior on the ISRS under very severe earthquakes.

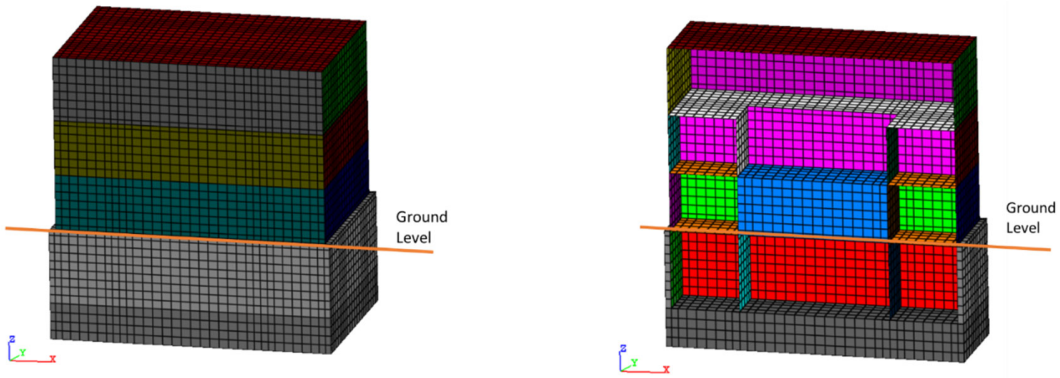

(a) Exterior view (b) Interior view

Figure 1. Sample building model for FSSI analysis

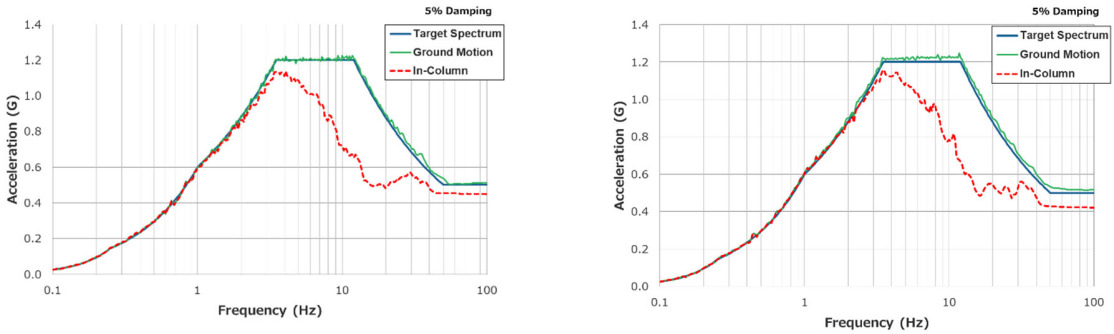

(a) X direction (b) Y direction

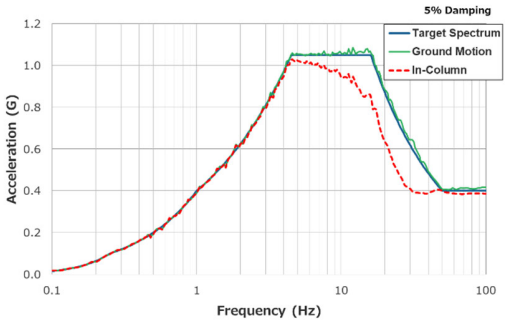

(c) Z direction

Figure 2. Seismic input motions

CASE STUDY FOR INELASTIC BEHAVIOR USING JAPANESE AND US CODES

In this study, the following three cases were used for the FSSI analyses with SC walls.

- Case 1: Elastic model with no SC wall concrete cracking based on Japanese design code
- Case 2: Inelastic model with concrete cracking and steel yielding based on Japanese design code
- Case 3: Elastic cracked model based on US design code

In Case 1, any inelastic effect including SC wall concrete cracking was not considered. The linear FSSI analysis with Case 1 was performed as reference in comparison with Cases 2 and 3 which consider inelastic effects due to concrete cracking.

In Case 2, the JEAC4618-2009 code was applied to determine the effective stiffness of the SC wall modeling. In this case, the trilinear backbone curves (BBC) considering both SC wall concrete cracking and steel yielding were applied to both in-plane bending moments and in-plane shear forces. The nonlinear FSSI analysis was performed using ACS SASSI Option NON which uses an efficient iterative hybrid frequency-time approach as described in detail elsewhere (Sato et al., 2024).

In Case 3, AISC N690-18 was applied to the SC modeling as the design code, for the comparison of inelastic effects with the Japanese code, JEAC4618. In the model, the concrete cracking effects were represented by reducing the shear stiffness and axial compression stiffness, on the assumption that concrete in all SC walls was cracked.

SC STRUCTURE WALL MODELING FOR NONLINEAR SSI PER JEAC4618-2009

The ACS SASSI Option NON iterative hybrid approach includes at each iteration two coupled analysis steps as follows (Sato et al., 2024):

Step1: Perform an equivalent-linear SSI analysis in complex frequency via the SASSI approach to compute the structural displacements for each nonlinear SC or RC wall at each floor level, and then,

Step 2: Perform a hysteretic time-domain analysis for each SC or RC wall loaded with the SSI displacements at each floor level from Step 1, to compute the in-plane shear and bending nonlinear wall responses using the standard-based BBC equations and the appropriate hysteretic models from the available software library.

The iterated equivalent-linear stiffness and damping for each SC wall were computed based on the time domain nonlinear responses using either a constant or a variable maximum displacement reduction factor (DRF) applied at each SSI iteration. Based on the nuclear building model layout, the SC walls were divided into eight nonlinear sub-models. The selected eight SC wall nonlinear sub-models are shown in Figure 3. The exterior SC wall sub-models, and the interior SC wall sub-models are shown in Figure 4 and 5, respectively. The partition of each nonlinear wall sub-model at each floor level is named “panel”. Figure 4 and 5 also shows the wall panel numbering.

Inelastic Modeling based on JEAC4618 Design Code

The nonlinear modeling if the SC wall panels was performed based on the following nonlinear characteristics.

For shear deformation, the Maximum Point-Oriented (PO) shear hysteretic model in JEAC4618-2015 is selected. For bending deformation, the Maximum Point-Oriented Degrade-Trilinear bending hysteretic model is selected.

Shear BBC

The shear force Q - shear strain γ relationship is represented using three breaking points as shown below.

1st breaking point for shear force (concrete cracking):

$$Q_1 = \left(A_c + \left(\frac{G_s}{G_c}\right) \cdot A_s\right) \cdot \sqrt{0.31\sqrt{F_c} \cdot \left(0.31\sqrt{F_c} + \sigma_v\right)} \quad (1)$$

$$\gamma_1 = \left(\frac{\tau_{cr}}{G_c}\right) \quad (2)$$

A_i: Cross-sectional area (i=c: concrete, i=s: steel) (mm^2)
F_C: Compressive strength of concrete (N/mm^2)
σ_v: Vertical axial compressive stress (positive for compression, N/mm^2)
G_c: Shear modulus of concrete (N/mm^2).

2nd breaking point for shear force (steel yielding)

$$Q_2 = \frac{\left(K_\alpha + K_\beta\right)}{\sqrt{\left(3K_\alpha^2 + K_\beta^2\right)}} \cdot A_s \cdot \sigma_y \quad (3)$$

$$\gamma_2 = \frac{Q_2}{\left(K_\alpha + K_\beta\right)} \quad (4)$$

where,

$$K_\alpha = A_s \cdot G_s \quad (5)$$

$$K_\beta = \left(\frac{4}{\left(A_c \cdot E_c'\right)} + \frac{2(1-\nu_s)}{\left(A_s \cdot E_s\right)}\right) \quad (6)$$

σ_y: Yield stress of steel plate (N/mm^2)
E_c': Young modulus of cracked concrete. The value can be 0.7 times the original concrete young's modulus (N/mm^2).
G_s: Shear modulus of steel (N/mm^2)
ν_s: Poisson ratio of steel.

3rd breaking point for shear force (ultimate strength)

The shear stress Q_3 and the shear strain γ_3 for ultimate state at point 3 of shear BBC are defined as below.

$$Q_3 = A_c \cdot \sqrt{\left(A_s/A_c \cdot \sigma_y \cdot \nu_1 \cdot F_c\right)} \quad (7)$$

$$\nu_1 = 0.7 - F_c/200 \quad (8)$$

Bending BBC

The bending moment M - curvature ϕ relationship is represented using three breaking points as below.

1st breaking point for bending moment (concrete cracking):

$$M_1 = Z_e(f_t + \sigma_v) \quad (9)$$

$$\phi_1 = \frac{M_1}{E_c \cdot I_e} \quad (10)$$

where

Z_e: Effective section modulus including steel plate (mm^3)
$f_t = 0.38\sqrt{F_C}$: Flexural tensile strength of concrete (N/mm^2)
E_c: Young's modulus of concrete (N/mm^2)
I_e: Equivalent section moment of inertia including steel plate (mm^4)
σ_v: Vertical axial compressive stress (positive for compression, N/mm^2)

2nd breaking point for bending moment (steel yielding):
The bending moment M_2 and the curvature ϕ_2 for yielding at point 2 are defined as below.

$$M_2 = M_y \quad (11)$$

$$\phi_2 = \phi_y \quad (12)$$

where
M_y: Moment by tensile stress at yielding point of steel plate (N-mm)
ϕ_y: Curvature by tensile stress at yielding point of steel plate (1/mm)

3rd breaking point for bending moment (ultimate strength):

The bending moment M_3 and the curvature ϕ_3 for ultimate state at point 3 are defined as below.

$$M_3 = M_u \quad (13)$$

$$\phi_3 = \mathrm{Max}(0.004/X_{nu}, 20\phi_2) \quad (14)$$

where
M_u: Full plastic moment (N-mm)
X_{nu}: Distance from compression edge to neutral axis at full plastic moment (mm)

The effective flange width for each SC wall panel is calculated based on the AIJ Standard for Structural Calculation of RC Structures (AIJ RC, Architecture Institute of Japan, 2018). These values are used for calculating section modulus, Z_e for each panel.

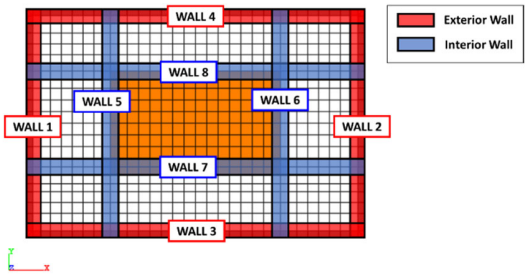

Figure 3. Nonlinear SC wall sub-models in top view

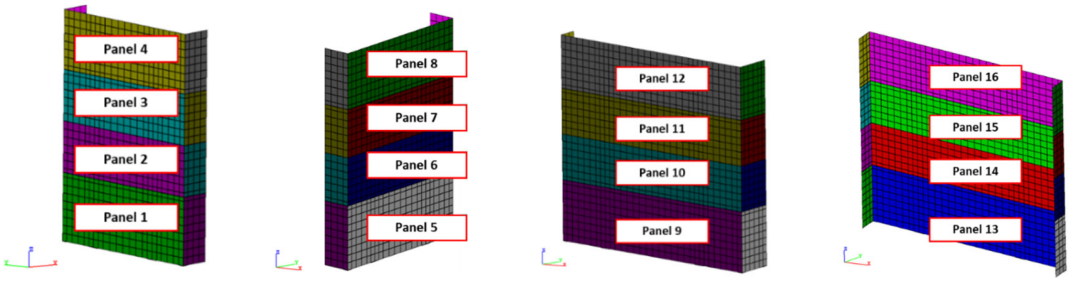

(a) Wall 1 (b) Wall 2 (c) Wall 3 (d) Wall 4

Figure 4. Exterior SC wall panels

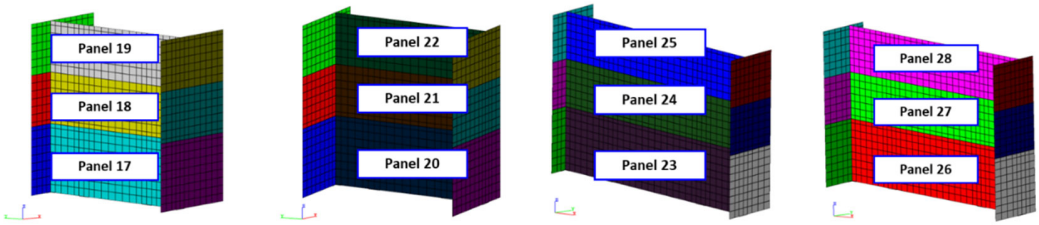

(a) Wall 5 (b) Wall 6 (c) Wall 7 (d) Wall 8

Figure 5. Interior SC wall panels

SC STRUCTURE WALL MODELING FOR LINEAR SSI PER AISC N690

According to AISC N690, the concrete cracking conditions can be considered for each effective stiffness. The out-of-plane bending effective stiffness can be expressed as below.

$$(EI)_{eff} = E_s I_s + c_2 E_c I_c \quad (15)$$

where
c_2: parameter for setting effecting bending stiffness
E_i: Young's modulus (i=c: concrete, i=s: steel)

Axial compression stiffness with concrete cracking is calculated based on the US practice (NuScale Power, 2021).

$$E_m A_{eff} = E_s A_s + E_c A_c/2 \quad (16)$$

Then, the effective stiffness E_m can be calculated by the following equation.

$$E_m = \frac{(EI)_{eff}}{I} = \frac{(EI)_{eff}}{A_{eff} T_m^2/12} = \frac{12(EI)_{eff}}{A_{eff} T_m^2} \quad (17)$$

To establish the two equations (15) and (16), the effective stiffness T_m can be formulated by the following.

$$T_m = \sqrt{\frac{12(EI)_{eff}}{E_m A_{eff}}} \quad (18)$$

As for the in-plane shear stiffness, the following equations are applied as per AISC N690 on the assumption that the stress is more than double of the allowable limit for concrete cracking.

$$(GA)_{cr} = 0.5\bar{\rho}^{-0.42} G_s A_s \quad (19)$$

where
G_S: Shear modulus of steel
$\bar{\rho}$: Stiffness-adjusted reinforcement ratio.

Then, the effective stiffness of shear modulus, G_m can be expressed as below.

$$G_m = (GA)_{cr}/T_m \quad (20)$$

The effective Poisson ratio for V_m can be expressed as below, using the material isotropic relationship.

$$V_m = \frac{E_m}{2G_m} - 1 \quad (21)$$

SUMMARY OF SC WALL EFFECTIVE STIFFNESS FOR JAPANESE AND US CODES

The computed effective stiffnesses based on Japanese and US codes is summarized in Table 1. It should be noted that while Japanese JEAC 4618 code requires nonlinear SSI analysis for SC structures, the US AISC N690 code requires only linear SSI analysis with reduced effective stiffnesses for shear and bending deformation.

For describing nonlinear SC wall behavior, the Japanese JEAC 4618 code considers trilinear BBC curves including the concrete cracking, steel yielding and ultimate points for in-plane shear deformation, whereas the US AISC N690 code considers only a bilinear BBC including the concrete cracking and steel yielding points, with yielding point being considered also as the ultimate point.

A special modeling aspect is that US code considers the effective stiffness for out-of-plane bending deformation, while Japanese code does not considers the effective stiffness for out-of-plane bending deformation. It should be noted that for RC structures, usually, all design codes, including Japanese and US codes, consider for seismic analysis only the in-plane shear and the in-plane bending hysteretic effects for the RC walls along each horizontal input motion direction. The consideration of the out-of-plane bending stiffness degradation of SC walls for the seismic analysis is particular to the US AISC N690 code.

Furthermore, it should be noted that the reduction of the effective stiffness for out-of-plane bending effects affects the SC wall axial stiffness. This is a conceptual difference between the two codes for SC structure wall modeling which directly affects vertical responses as shown in results of the next section.

The material properties applied to each case is shown in Table 2. For SC walls, steel face plates with 10 mm were assumed to be applied to concrete walls with thickness of 500 mm.

The equivalent Young's modulus and wall thickness were calculated on the assumption that the following material properties were applied to SC structures:

- Concrete density: 24 kN/m^3
- Concrete Young's modulus: 25.7 GPa
- Concrete Poisson ratio: 0.2
- Steel density: 78 kN/m^3
- Steel Young's modulus: 205 GPa
- Steel Poisson ratio: 0.3
- Thickness of steel plate: 10mm.

Table 1: Summary of Comparison of Effective Stiffness between Japanese and US standards

Item	Japanese Standard (Case 2)	US Standard (Case 3)
Analysis Method	Effectively iterative equivalent linear analysis (3 times)	Equivalent linear analysis (with reduced stiffness)
Out-of-plane Stiffness	Effective bending stiffness is not considered.	Effective bending stiffness with concrete cracking is considered
In-plane Stiffness	Trilinear BBCs are applied to shear and bending stiffness	Effective stiffness with concrete cracking is considered for shear and bending
Damping Ratio of SC	Hysteretic damping is added to initial elastic damping	Increased 5% damping is applied when concrete cracking is considered.

Table 2: Material Properties

Material Parameter		Case 1 (Elastic Uncracked JEAC4618)	Case 2 (Inelastic Cracked, JEAC4618)	Case 3 (Elastic Cracked, AISC N690)
SC wall	Density of SC	26.66 kN/m^3	26.66 kN/m^3	21.87 kN/m^3
	Young's modulus	32.87 GPa	Calculated by BBC for each wall panel	17.17 GPa
	Poisson ratio	0.223		0.299
	Damping ratio	3%	Hysteretic damping	5%
	Thickness	0.5 m	0.5 m	0.598 m (Equivalent thickness)
RC floor slab	Density	24 kN/m^3		
	Young's modulus	25.7 GPa		
	Poisson ratio	0.2		
	Damping ratio	5%		

COMPARATIVE RESULTS AND DISCUSSIONS

For the Case 2 based on Japanese code, with inelastic SC wall behavior for shear and bending deformations, the computed equivalent moduli and damping ratios are shown in Figures 6 and 7, respectively. With regard with the elastic moduli in the embedded walls at the lowest level (Panels 1, 5, 9, 13, 17, 20, 23 and 26 in Figures 4 and 5), no decrease was observed in the elastic moduli obtained by shear forces even after iterative computations, whereas the elastic moduli obtained by bending moments were decreased for exterior walls. This implies that for the SC wall panels of the embedded walls in contact with the lateral soil, the shear deformations were highly reduced.

The elastic moduli ratios applied to 3D Finite Element model were calculated at each iteration by combining the shear and bending interaction effects using an ellipsoidal shape interaction curve between

the equivalent stiffnesses. It should be noted that ACS SASSI Option NON can also use orthotropic materials for SC wall modeling, so that the shear and bending effects are independently affecting the Young's and shear elastic moduli at each iteration. Usually, the differences in end results are negligible. (Ghiocel Predictive Technologies, Inc., 2024).

When comparing elastic moduli of the three cases, it was confirmed that elastic moduli of Case 3 (Elastic cracked model based on US code) were smaller than Case 2 (Japanese code, nonlinear SSI with degraded concrete SC wall stiffness). However, the equivalent moduli of the Case 3 can be comparable to that of Case 2 due to the increase of equivalent wall thickness of shell elements.

With regard to the damping ratios, it was confirmed that the equivalent damping ratios were increased at the panels which have reduced elastic moduli. The damping ratios for Case 2 were larger than those of Case 3, except that some of other panels in Case 2 had the initial damping of 3% without any concrete cracking. In the SSI analysis with 3D FE model in frequency domain, maximum damping ratios between shear-damaged damping and bending-damaged damping were applied at each panel.

To compare seismic responses among the three analysis cases, ISRS at the nodes presented in Figure 8 were generated. The ISRS for each node and each direction are shown in Figure 9 through 14. With regard to X direction, no remarkable differences among three cases were shown. However, with regard to Y direction, some differences among the three cases were noticeable. For both Node 10444 and 8738, the responses in cracked concrete models, in Cases 2 and 3, were shifted to the lower frequency side, comparing with the responses in the uncracked model, Case 1.

For Node 10444 in Y direction, some differences of the ISRS appeared at the frequency range exceeding 20 Hz. For Z direction, obvious differences of the ISRS between Case 2 and 3 were observed. It was confirmed that the US design code approach in Case 3 has a tendency to change the axial SC wall stiffnesses due to assumed cracked concrete in comparison with uncracked concrete condition of Case 1..

The ISRS in Case 3 were reduced at around 10 Hz when comparing with Cases 1 and 2. However, the vertical ISRS in Case 3 at 9.5 Hz and 13-14 Hz were larger than those in Case 2. This phenomenon is considered to be due to the large stiffness change of the SC shear walls.

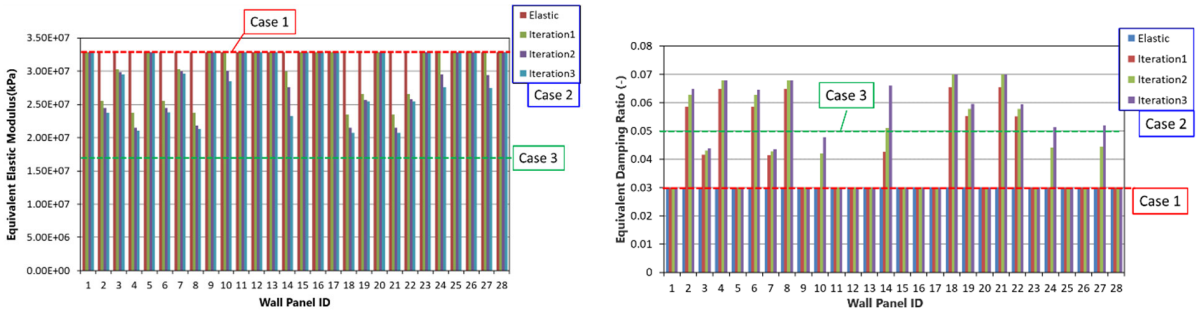

(a) Equivalent elastic moduli (b) Equivalent damping ratios

Figure 6 Equivalent elastic moduli and damping ratios for shear deformation

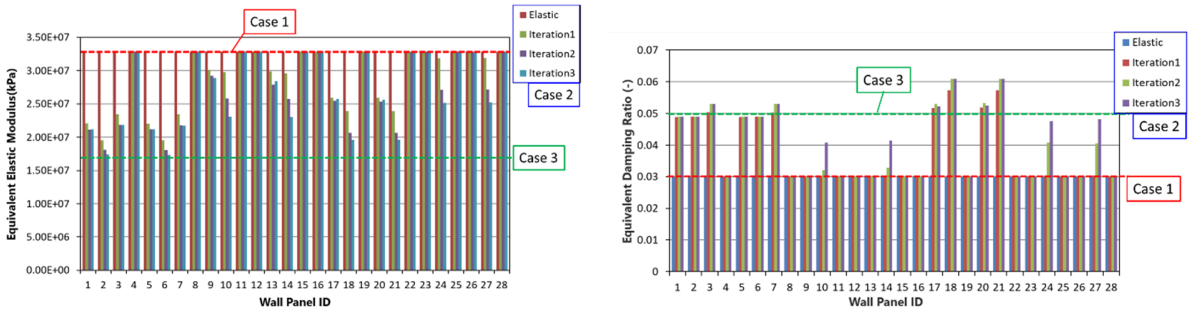

(a) Equivalent elastic moduli (b) Equivalent damping ratios

Figure 7 Equivalent elastic moduli and damping ratios for bending deformation

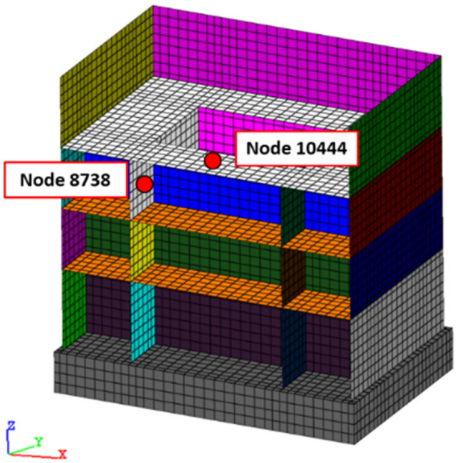

Figure 8. Node positions

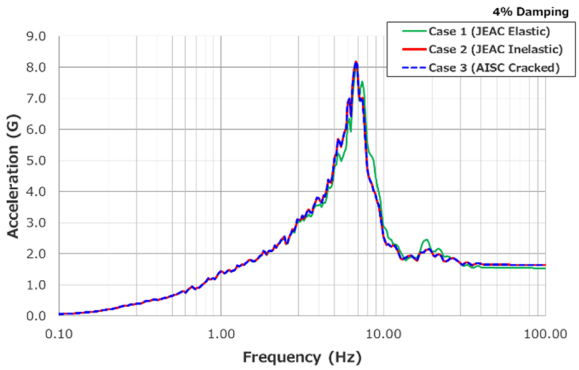

Figure 9, ISRS at Node 10444 (X direction)

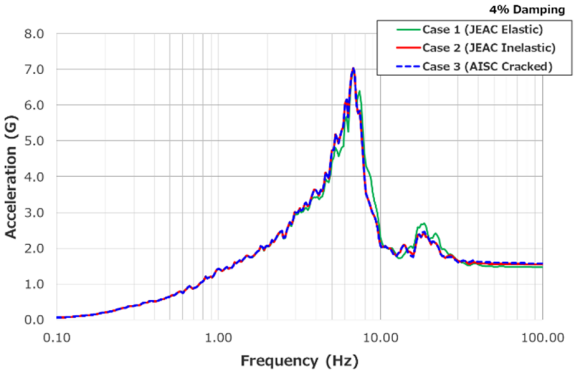

Figure 10. ISRS at Node 8738 (X direction)

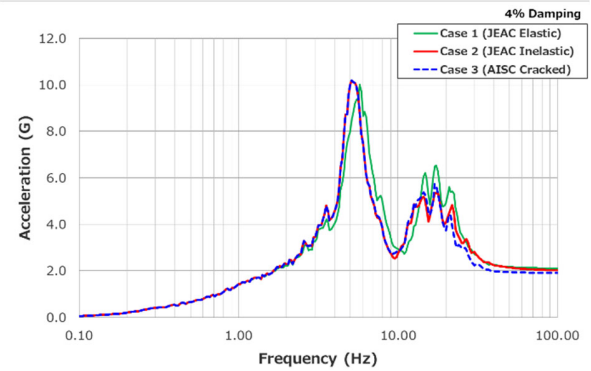

Figure 11. ISRS at Node 10444 (Y direction)

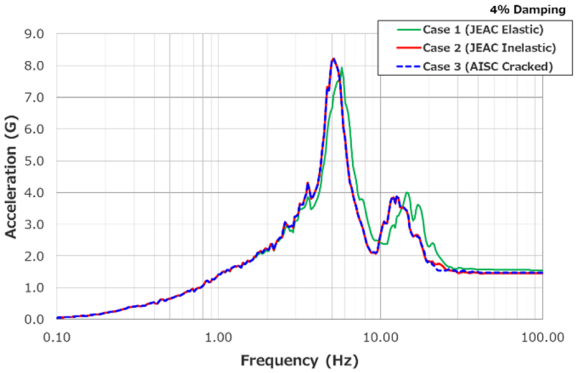

Figure 12. ISRS at Node 8738 (Y direction)

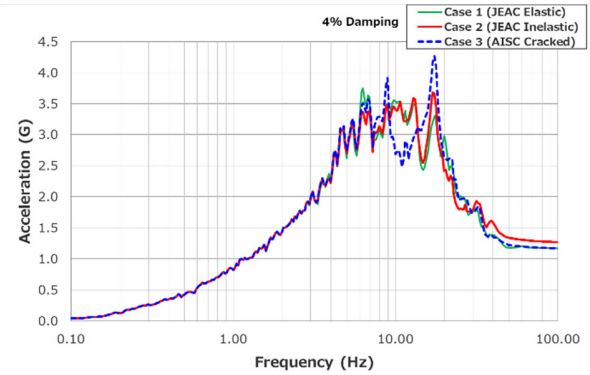

Figure 13. ISRS at Node 10444 (Z direction)

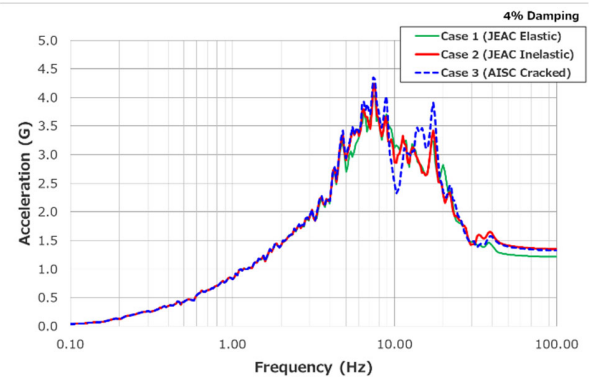

Figure 14. ISRS at Node 8738 (Z direction)

CONCLUSIONS

The SC structure SSI analysis results showed the different seismic responses depending on the modeling approaches of the inelastic deformation of the SC walls.

The comparison of ISRS between elastic and inelastic SSI analysis model revealed that the peak responses of ISRS can be shifted to lower frequency side due to the concrete cracking effect of the building structure for one horizontal direction. For horizontal directions, it was confirmed that the inelastic SC model based on the Japanese design code provides similar responses as the elastic SC model with cracked concrete based on the US design code. For vertical direction, there is an obvious difference in the ISRS shape between the Japanese code basis SSI model and the US code basis SSI models, due to the different axial stiffness of SC walls.

To obtain larger differences the two different design code modeling of SC walls, more severe earthquakes need to be considered. The effect of degraded stiffness beyond the yielding point of steels in the Japanese design code will need to be examined as a separate study.

REFERENCES

American Institute of Steel Construction (2018), ANSI/AISC N690-18, Specification for Safety-Related Steel Structures for Nuclear Facilities.

Ghiocel Predictive Technologies, Inc., ACS SASSI NQA Version 4.3.7 (IKTR3.7) Including Options A-AA and NON User Manual Revision 10, November 30, 2023.

NuScale Power LLC., NuScale Standard Plant Design Certification Application, Revision 5, (2020).

NuScale Power LLC., TR-0920-71621-NP Revision 1, Licensing Topical Report Building Design and Analysis Methodology for Safety-Related Structures, October 2021.

Japan Electric Association, Nuclear Standards Committee (2009), JEAC4618-2009, Technical Code for Seismic Design of Steel Plate Reinforced Concrete Structures: Buildings and Structures, Japanese Electric Association.

Sato, Y., Ghiocel, D. M., Kataoka, S., Sato, S., and Morimoto, Y. (2023). *Study on Fluid-Structure-Soil-Interaction (FSSI) Effects for A Deeply Embedded Nuclear Facility with A Large-Size Pool Under Severe Earthquakes. Part 1: Linear SSI.* SMiRT27 Conference, Division III, Yokohama, Japan, March 3-8, 2024.

Sato, Y., Ghiocel, D. M., Kataoka, S., Sato, S., and Morimoto, Y. (2023). *Study on Fluid-Structure-Soil-Interaction (FSSI) Effects for A Deeply Embedded Nuclear Facility with A Large-Size Pool Under Severe Earthquakes. Part 2: Nonlinear SSI.* SMiRT27 Conference, Division III, Yokohama, Japan, March 3-8, 2024.